IX International Conference on Computational Methods in Marine Engineering
MARINE 2021
I.M. Viola and F. Brennan (Eds)

DESIGN OPTIMISATION OF PRESSURE VESSEL BUNDLES FOR OFFSHORE HYDRO-PNEUMATIC ENERGY STORAGE USING A SMART DESIGN SOFTWARE

CHARISE CUTAJAR[*], TONIO SANT[*†], ROBERT N. FARRUGIA[†] AND DANIEL BUHAGIAR[‡]

[*] Department of Mechanical Engineering,
University of Malta,
Msida MSD 2080, Malta
e-mail: info@um.edu.mt, web page: http://www.um.edu.mt

[†] Institute for Sustainable Energy
University of Malta,
Marsaxlokk MXK1531, Malta
e-mail: ise@um.edu.mt, web page: http://www.um.edu.mt/ise

[‡] FLASC B.V.
Paardenmarkt 1, 2611 PA,
Delft, The Netherlands
e-mail: info@offshoreenergystorage.com, web page: www.offshoreenergystorage.com

Key words: Pressure Vessels, Offshore, Energy Storage, Optimisation

1 INTRODUCTION

With the gradual shift towards renewable energy sources (RES), the ocean is now being recognised as an enormous natural source of clean energy which can supply power ranging from ocean thermal energy conversion (OTEC) to tidal and wave energy. Wind turbines have also been taken out at sea to benefit from the more favourable wind conditions offshore. In fact, offshore wind energy has now become the most technically advanced marine-based technology. The total global installed offshore wind capacity reached 29 Giga-Watts (GW) by the end of 2019, which has been reported to be the best year for the offshore wind industry to date [1].

The main drawback in the field is that the power harnessed from the wind is highly erratic due to the stochastic nature of the resource, which can have detrimental effects on the stability, operational security, reliability and efficiency of power systems. In light of the present challenge and the large-scale penetration of offshore wind power, energy storage systems (ESSs) have been standing out in the ability to increase flexibility, control intermittence and guarantee a back-up system to electrical networks. In fact, several novel energy storage concepts are emerging on the market, including those specifically designed for integration offshore. The technologies range from electro-chemical solutions such as lithium-ion batteries [2] to pumped hydro-electric storage and underwater compressed air energy storage

(UWCAES) systems. Examples of the latter two types include the StEnSea [3] and the Energy Bags [4] concepts, respectively. Recently, hydro-pneumatic energy storage (HPES) systems have been considered for offshore use due to various advantages, including the ability to deploy in a fully subsea environment which can act as a natural heatsink, long lifetimes and safe operation resulting from low fire risk.

This paper focuses on the design optimisation of pressure vessels (PVs) used in offshore HPES systems. Three different case studies are analysed with respect to the design and operational parameters to allow for convergence towards the optimum values. The tests were performed using a smart software tool *SmartPVB*, which has been developed in-house specifically for the given purpose. The case studies investigated are highlighted in the next section. Section 3 presents a mathematical model on which the numerical model outlined in Section 4 is based. The methodology adopted is outlined in Section 5, followed by the results generated from the software in Section 6. The conclusions and new knowledge gained from this study are then summarised in Section 7.

2 HPES SYSTEM CONFIGURATIONS

HPES technologies are mechanical ESSs operating solely on fluids and available in closed- and open-cycle circuits. Both concepts operate in a similar manner whereby energy is stored by pumping an incompressible liquid which acts to compresses a gas inside a chamber. To discharge, the gas is allowed to expand, expelling the liquid at high pressures, driving a turbine or hydraulic motor to release the stored energy. The key difference between both configurations is that the open-cycle system provides an additional chamber for the compressed air, thus limiting pressure fluctuations and achieving relatively higher energy densities [7].

The two closed-cycle configurations investigated in this paper are presented in Figure 1. Both systems are identical, comprising a seabed-mounted Pressure Vessel Bundle (PVB) of multiple PVs, anchored at different sea depths. Alternatively, Figure 2 illustrates the open-cycle HPES system which is specifically that of the FLASC concept [5]. The latter is a novel and patented open accumulator developed by the University of Malta which can be integrated within a floating wind turbine support platform, thus exploiting the internal volume within the substructure and reducing the size requirements of the infrastructure installed on the seabed.

The Floating Liquid-piston Accumulator using Seawater under Compression (i.e. FLASC) is based on two interconnected PVBs. The seabed-mounted lower bundle serves as an accumulator connected to a hydraulic circuit. The latter provides or extracts hydraulic power to and from the system as required, via the liquid-piston mechanism. The upper bundle integrated within the Floating Offshore Wind Turbine (FOWT) substructure such as a spar, absorbs the pressure fluctuations that result from the thermodynamic compression and expansion processes during operation. Both bundles are interconnected via a pneumatic-umbilical. FLASC may also be utilised for additional offshore processes and/or activities, thus leveraging existing supply chains and infrastructure [5].

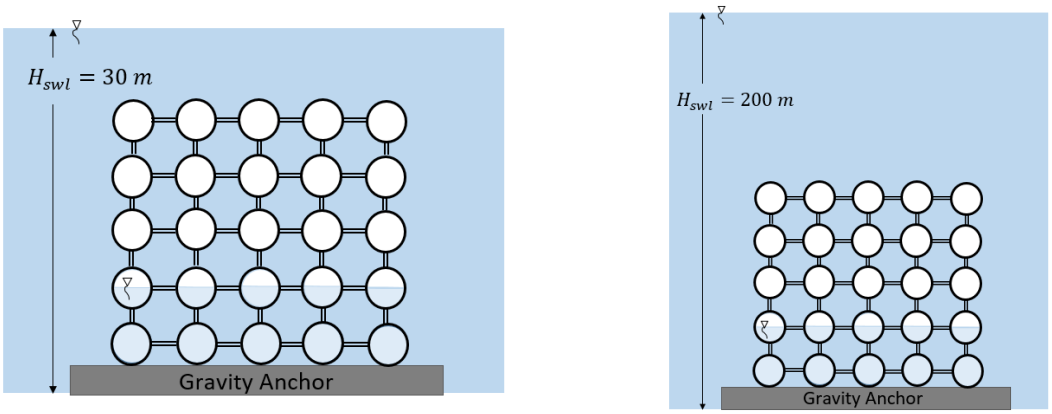

Figure 1: Seabed-mounted closed-cycle HPES system
a) deployed at 30-m sea depth b) deployed at 200-m sea depth

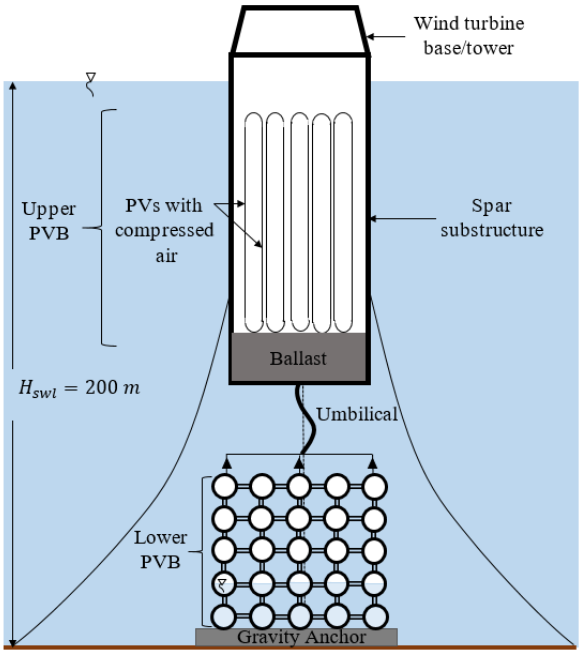

Figure 2: Open-cycle FLASC HPES system

3 THEORETICAL REVIEW

This section presents the background theory forming the basis for the software tool used in this study. Design parameters and computations are all based on the Unfired Pressure Vessels – Part 3: Design, SM EN Standard (SM EN 13445-3:2014) [6]. The mathematical model assumes (i) steels (except for castings) with a minimum rupture elongation, as given in the relevant technical specifications for the material below 30% as defined in Clause 6.2 of [6]; (ii) hemispherical-ended PVs and (iii) thin-walled structures.

3.1 Structural analysis

The geometry of one PV in a bundle of identical PVs is illustrated in Figure 3. The overall length of the PV, L_{pv}, is defined as the length from end-to-end of the vessel, including the two hemispherical ends. Therefore, the length L of the cylindrical section may be computed using Eq. (1) where D_o is the external diameter of the vessel.

$$L = L_{pv} - D_o \tag{1}$$

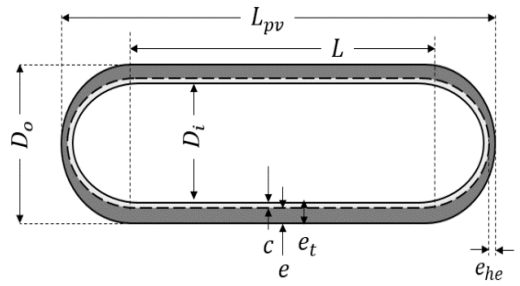

Figure 3: Geometry of a single PV

The program is only valid for PVs under a net internal pressure and hence, the wall thickness required to sustain the pressure loadings experienced by the structure is determined in accordance with the SM EN 13445-3:2014 Standard, Clause 7.4 [6], so that:

$$e = \frac{p_{net} D_o}{2(10^6) z f_d + p_{net}} \tag{2}$$

In Eq. (2), p_{net} is the net pressure, calculated as the difference between the design pressure p_d and the maximum operating pressure p_{max}. With reference to the Pressure Equipment Directive (PED) [7] and other literature sources [8], it is suggested that p_d is equivalent to p_{max} multiplied by a factor of at least 1.1 to provide a safety factor for design purposes. Moreover, z and f_d in Eq. (2) are the joint coefficient and nominal design stress respectively and are defined in the standard [6]. Similar to Eq. (2), the thickness at the hemispherical ends is given in Clause 7.5.2 of [6] and is roughly half that required for the cylindrical shell. The total thickness of the vessel e_t, is uniform throughout and is computed using Eq. (3), where c is an additional thickness to cater for corrosion during its lifetime, such that:

$$e_t = e + c \tag{3}$$

From the dimensions marked in Figure 3, the volumetric capacity of the PV is given by Eq. (4), where the first term is the volumetric capacity of the cylindrical part whilst the second term is the volumetric capacity of both hemispherical ends:

$$V_{pv} = \frac{\pi L D_i^2}{4} + \frac{\pi D_i^3}{6} \tag{4}$$

Applying thin cylinder theory, the volume of material (i.e. steel) required for one PV may be determined from Eq. (5), where D_i is the internal diameter of the PV:

$$V_{st} = \left[\pi L e_t \left(\frac{D_o + D_i}{2}\right)\right] + \left[\frac{\pi}{6}(D_o^3 - D_i^3)\right] \quad (5)$$

The total mass of the PVB with a quantity Q of PVs is computed using Eq. (6) by adding the total mass of steel ($\rho_{st}V_{st}$), the mass of fluids (i.e. liquid seawater and air) inside the vessels and any additional mass allowance, m_{ad}, due to welds and other auxiliary components.

$$m_{pvb} = Q\left(\rho_{st}V_{st} + m_{air} + m_{liq} + m_{ad}\right) \quad (6)$$

3.2 Hydrostatic analysis

The hydrostatic static stability of the HPES system is determined using Archimedes' principle which, in mathematical terms may be expressed using Eq. (7). The left-hand side term of the equation represents the empty weight of the PVB and the weight of the concrete anchor ($m_c g$) which is required to secure the system in place (refer to Figures 1 and 2). The weight when empty is considered to ensure hydrostatic stability at all times even during the deployment stage, prior to operation. The term on the right-hand side is the total upthrust of the system multiplied by an anchoring safety factor, $f_{s,hyd}$. The latter shall be determined based on multiple factors including, but not limited to the seabed conditions and hydrodynamic loads.

$$\left(Qm_{e,pv} + m_c\right)g = \rho_{sw}V_d g f_{s,hyd} \quad (7)$$

Consequently, the volume of concrete required to keep the structure anchored underwater is computed using Eq. (8) where V_d is the volume of seawater displaced by the PVB.

$$V_c = \frac{\left(\rho_{sw}f_{s,hyd}V_d\right) - \left(Qm_{e,pv}\right)}{\rho_c - \rho_{sw}f_{s,hyd}} \quad (8)$$

3.3 Thermodynamic analysis

The thermodynamic model for the HPES system is based on the assumptions that: (i) the pressurised gas inside the system is air that can be treated as an ideal (i.e. perfect) gas; (ii) the compressed air is dry; (iii) frictional heating is negligible and the pressurised air is initially in thermal equilibrium with the surrounding water and; (iv) seawater is an incompressible fluid. In accordance with the second assumption listed, the mass of air that one PV occupies at any state of charge may be determined from the ideal gas equation. The nature of the compression and expansion processes is governed by the ratio of the maximum pressure, p_{max} to the pre-charged air pressure, p_{pre} and is known as the pressure ratio r_p, which may also be expressed in terms of the air volumetric ratio of compression/expansion r_v, as follows:

$$r_p = \frac{p_{max}}{p_{pre}} = \left(\frac{V_1}{V_2}\right)^n = r_v^n \quad (9)$$

where n is the polytropic index and the subscript 1 denotes the fully discharged state. Subscript 2 refers to the fully charged state. Table 1 summarises the air and liquid volumes inside a seabed-mounted PVB with a number Q of PVs, at both extreme states of charge. The fluid volumes for the FLASC HPES system are presented in Table 2. The terms V_L and V_U are

the total volume capacities of the lower and upper PVBs respectively, and are related through r_v as per Eq. (10).

Table 1: Air and liquid volume in the PVB at different states of charge for a HPES system on the seabed

	Fully discharged - State 1	**Fully charged - State 2**
V_{air} (m^3)	QV_{pv}	$\frac{QV_{pv}}{r_v}$
V_{liq} (m^3)	0	$QV_{pv}\left(1-\frac{1}{r_v}\right)$

Table 2: Air and liquid volume in PVBs at different states of charge for the FLASC model

	PVB	**Fully discharged - State 1**	**Fully charged - State 2**
$\boldsymbol{V_{air}}$ **(m^3)**	Lower	V_L	0
	Upper	V_U	V_U
$\boldsymbol{V_{liq}}$ **(m^3)**	Lower	0	V_L
	Upper	0	0

$$r_p = r_v = \frac{V_1}{V_2} = \frac{V_L + V_U}{V_U} = \frac{V_L}{V_U} + 1 \tag{10}$$

The size of the storage vessels determines the storage capacity of the system, which is directly attributed to the thermodynamic work done in compressing and expanding air during charging and discharging, respectively. For the isothermal thermodynamic process considered in this study, the polytropic index n equates to unity, and the work done is given by:

$$W_{iso} = p_{max}V_2 ln(r_v) - p_{hyd}V_2(r_v - 1) \tag{11}$$

The second term in Eq. (11) is the work done against the hydrostatic pressure, p_{hyd}. Eq. (12) is used to convert the work done (in Joules) into what can be assumed to be the ideal energy storage capacity, expressed in kilowatt-hours (kWhs):

$$E = \frac{W_{iso}}{3600(10^3)} \tag{12}$$

4 COMPUTATIONAL MODEL

The software tool *SmartPVB* caters for both closed- and open-cycle HPES systems. The equations presented in Section 3 have been arranged in chronological order to be solved algebraically. In a single run, the user can test for different numbers of PVs, PV outer diameters and operating pressure ratios, simultaneously. Structural, hydrostatic and thermodynamic solutions are obtained for all test values. An optimisation algorithm stores all computation results and identifies the minimum material requirements for the HPES system together with the constituent test conditions that resulted in the indicated optimum result.

5 METHODOLOGY

Tests were performed to analyse the similarities and differences between three different case studies. The energy storage capacity was kept fixed at 10 MWh for the following scenarios:

a. seabed-mounted HPES system arranged in a 5 by 5 PV configuration at a sea depth of 30 m (refer to Figure 1 (a));
b. seabed-mounted HPES system arranged in a 5 by 5 PV configuration at a sea depth of 200 m (refer to Figure 1 (b));
c. FLASC HPES system (refer to Figure 2) comprising of:
   i. a lower PVB arranged in 5 by 5 PV configuration at a sea depth of 200 m;
   ii. an upper PVB with 95 PVs staggered within a wind turbine spar floater.

Parameters with values common to all tests and HPES configurations are summarised in Table 3. All tests were performed for pressure ratios ranging from 1.2 to 5 in increments of 0.1. The parameters whose values vary for the different configurations are presented in Table 4.

Table 3: Parameter values common to all the three case studies

Parameter	**Value**
Outer diameter, D_o (m)	0.914
Density of concrete, ρ_c (kg/m^3)	2450
Anchoring safety factor, $f_{s,hyd}$ (-)	1.1
Additional mass per PV, m_{ad} (%)	5
Material (i.e. steel) grade API-5L (-)	X70
Density of steel, ρ_{st} (kg/m^3)	7850
Yield strength, $R_{p,0.2/T}$ (MPa) [9]	483
UTS, $R_{m/20}$ (MPa) [9]	565
Corrosion allowance thickness, c (mm)	3
Polytropic index, n (-)	1
Horizontal clearance between PVs on the seabed, c_l (m)	$0.5D_o$
Design pressure, p_d (bar)	$1.1p_{max}$

Table 4: Parameter values specific to a given HPES system configuration

	On Seabed at 30 m	**On Seabed at 200 m**	**FLASC**	
	-	-	Lower PVB	Upper PVB
Number of PVs, Q (-)	25	25	25	95
Sea depth, H_{swl} (m)	30	200	200	0
Initial temperature of the compressed air, $T_{air,1}$ (°C) [10]	18.5	14.6	14.6	14.6

A spar-type substructure is considered for the FLASC HPES embodiment (refer to Figure 2). With reference to the Hywind, Scotland project [11] the spar outer diameter may be

approximated at 14.50 m. A readily available online algorithm [12] implementing the Circle Packing Theorem [13] was used to determine the number of cylinders with a D_o = 0.914 m (i.e. 36 inches) that can technically fit within such a spar. To allow for sufficient clearance between the PVs within the floater, the values of spar internal diameter and vessels outer diameter were set at 14 m and 1.25 m, respectively. The latter is 37% higher than the true physical dimension, leaving a gap of 67.2 cm between each vessel. The result from the online algorithm [12] implied that up to 95 cylinders could be accommodated in the floater.

6 RESULTS

6.1 General results at a fixed peak pressure

The results that follow are based on the inputs outlined in Tables 3 and 4. The optimal pressure ratio yielding minimum steel and concrete requirements for the seabed mounted PVB at 30 m depth was found to be 2.7, whereas for the other two configurations it was found to be 2.5. However, for the purpose of analysis at a common pressure ratio, the value of 2.5 was assumed for all the three cases.

Figure 4 shows the difference in PV length for the three configurations at a pressure ratio of 2.5 when operating at a peak pressure of 200 bar. Comparing the two seabed-mounted systems (Figure 1 (a) and (b)), a 15% increase in length is noted for the system installed in deeper waters (200m). With increasing sea depth and hence hydrostatic pressure, the net work decreases, as may be observed from Eq. (11). Therefore, more work is required to maintain a fixed energy storage capacity of 10 MWh. Furthermore, if the work done decreases, then the volume of air at full charge, and hence the volumetric capacity of the PVB, should increase for a fixed pressure ratio. Consequently, an increasing PV length with increasing sea depth is observed. Looking at the FLASC system, the length of PVs in the lower PVB on the seabed is significantly less than either of the seabed configurations. The length of FLASC's lower PVB decreases by up to 40% when compared to the equivalent seabed-mounted system at 200 m, and by 30% if the seabed-mounted configuration is deployed at 30 m. Consequently, the seabed area required diminishes by the same percentages as the remaining volumetric capacity of the FLASC HPES system is embedded in the floating substructure of a FOWT.

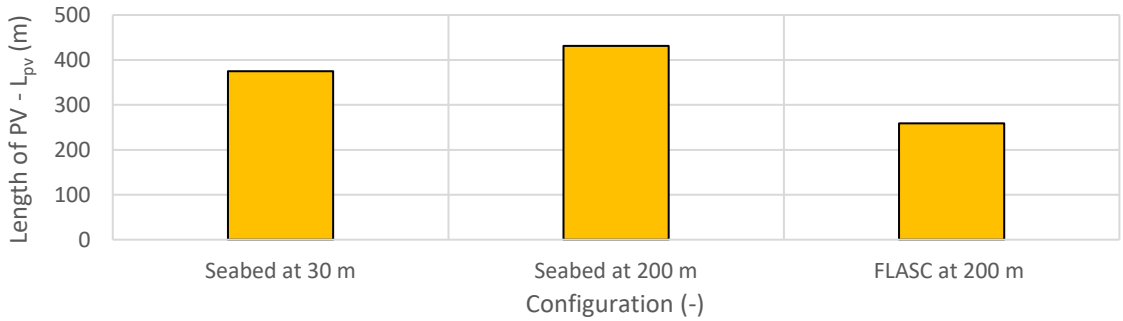

Figure 4: PV length for PVs resting on the seabed, for three different 10 MWh HPES systems at a pressure ratio of 2.5 and a peak pressure of 200 bar

Figure 5 shows that the configuration that makes use of least material is the seabed system anchored at 30 m below mean sea level (MSL). In such a case, the mass is 7% less than the same configuration mounted at a 200-m sea depth. The FLASC system requires the highest amount of steel, amounting to over 9,700 tonnes and equivalent to a 4% increase in the mass of material when compared to the seabed-mounted system at a depth of 200 m. Additional material is the result of fitting part of the HPES system's volume within the floater. A higher quantity of smaller vessels increases the number of hemispherical ends. Besides, the cylinders in the floater are always thicker than those on the seabed as they are housed in the substructure at atmospheric pressure and thus are not exposed to any hydrostatic pressure. For all three case studies, concrete is not required at a peak pressure of 200 bar as the PVs are able to self-anchor. Nonetheless, additional tests throughout the study not presented in this paper, suggest that concrete anchoring becomes essential when operating at peak pressures lower than 170 bar.

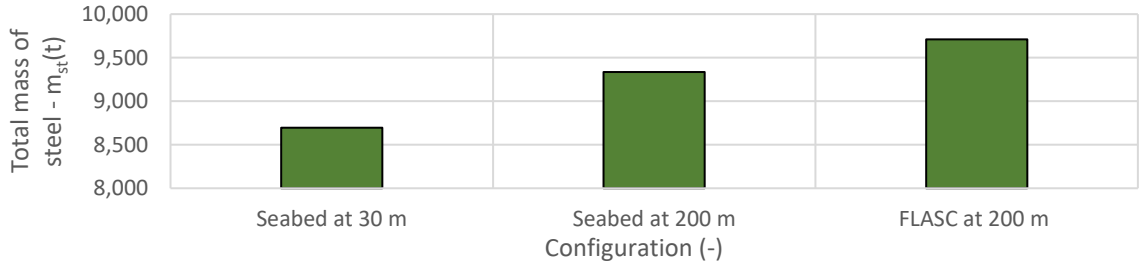

Figure 5: Mass of steel for three different HPES systems at a pressure ratio of 2.5 and a peak pressure of 200 bar

6.2 Results for different peak pressures

The testing conditions in Tables 3 and 4 were re-applied, yet the maximum operating pressure was varied between 150 bar and 400 bar in increments of 50 bar. Firstly, it is worth noting that changing the configuration and the peak operating pressure shift the optimal operating pressure ratio. The results are summarised in Table 5. For the modelled conditions, the optimal pressure ratio for the first case study remained fixed at 2.7, whereas for the other two configurations it varied between 2.4 and 2.6. Nonetheless, it can be concluded that in general, the minimum cost for an underwater HPES system deployed in waters up to a maximum depth of 200 m can be achieved at pressure ratios over 2.4, but never exceeding 3.0.

Table 5: Optimum operating pressure ratios for different configurations at different peak pressures

Peak operating pressure (bar)	Seabed configuration at 30 m below MSL	Seabed configuration at 200 m below MSL	FLASC configuration at 200 m below MSL
150	2.7	2.4	2.5
200	2.7	2.5	2.5
250	2.7	2.5	2.6
300	2.7	2.5	2.6
350	2.7	2.6	2.6
400	2.7	2.6	2.6

The variation of the PV length with peak pressure is presented in Figure 6. The decrease in length with higher operating pressure is due to the inversely proportional relationship between volumetric capacity and peak pressure, i.e. higher peak pressures result in more compact designs. Comparing both seabed systems to each other, the percentage difference in PV length ranges from 6 up to 22% when changing from shallow (i.e. at 30 m) to deeper waters (i.e. 200 m). The largest difference is realised at lower pressures and then becomes marginal with increasing operating pressures. The change in PV wall thickness is illustrated in Figure 7. Note that the thickest walls are recorded for the FLASC PVs in the spar floater, followed by the PVs when at a sea depth of 30 m and 200 m, respectively. This result reflects the effect of hydrostatic pressure in each case, which increases gradually from 0 bar, to 3 bar, and 20 bar respectively, hence reducing the net pressure experienced by the vessels.

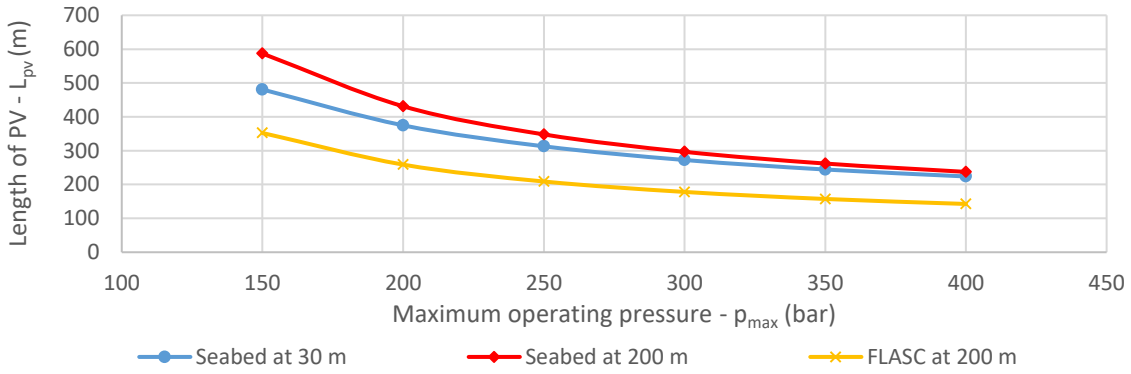

Figure 6: PV length variation with peak pressure for PVs resting on the seabed for three different HPES systems at a pressure ratio of 2.5

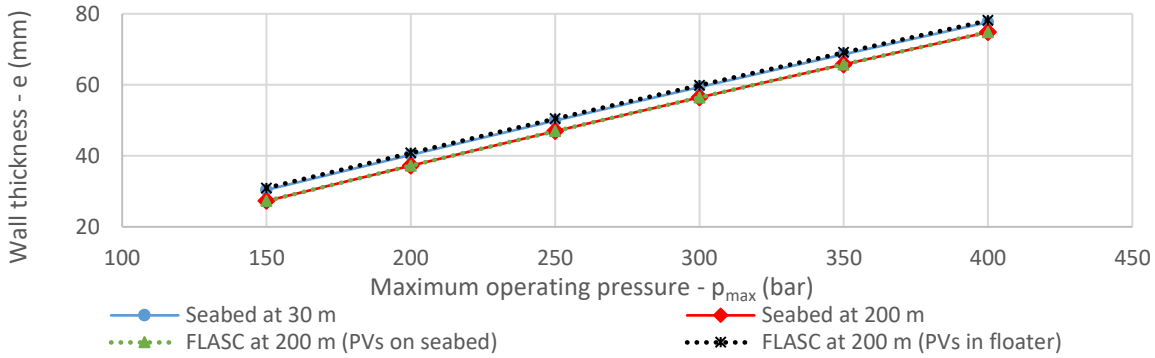

Figure 7: PV wall thickness variation with peak pressure for three different HPES systems at a pressure ratio of 2.5

A further result of interest is that of the variation of the total mass of steel with peak pressure which is given in Figure 8. It is evident that a minimum value is obtained between 150 and 200 bar for the seabed-mounted system at 30 m below MSL. The minimum result for the other two configurations is observed at higher peak pressures; at 250 bar for the closed-cycle system

at 200 m sea depth and at 300 bar for the FLASC HPES system. The qualitative characteristic of the three plots in Figure 8 results from the combined effect of decreasing PV length (refer to Figure 6) and increasing PV wall thickness (refer to Figure 7) for increasing peak pressures.

Higher material requirements will have a significant effect on the total cost of the system. Consequently, with regards to material costs (excluding installation costs), FLASC can prove to be the most expensive option at all tested peak pressures. Nonetheless, FLASC offers several unique advantages that will eventually reduce the lifetime cost of the technology. FLASC allows for higher energy densities and exceptional thermodynamic and round-trip efficiencies. Considering typical efficiencies of standard hydraulic pump-turbines, the round-trip efficiency can reach 70% [14]. With a smaller lower PVB, FLASC minimises its footprint on the seabed. Besides, a preliminary hydrodynamic study [15] has also suggested that the PVs in the floater act as ballast to the floating structure, contributing to a more statically stabilised system.

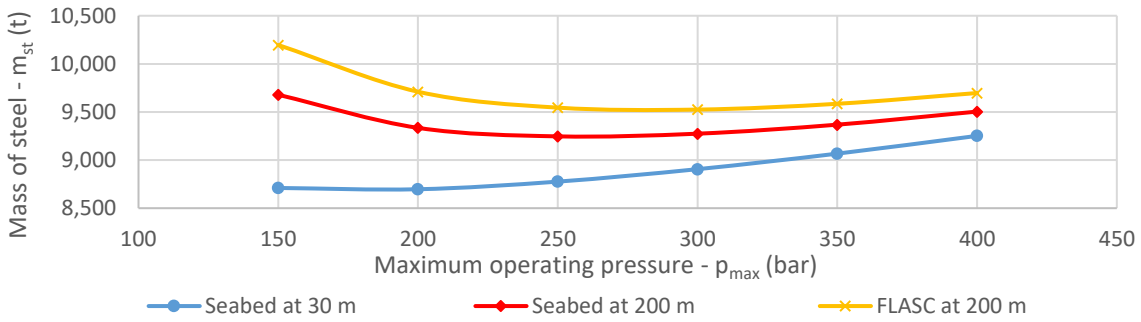

Figure 8: Mass of steel variation with peak pressure for three different HPES systems at a pressure ratio of 2.5

7 CONCLUSIONS

The paper has shed light on key design and operational parameters that can drive material reductions in offshore HPES systems. The main conclusions drawn from this study are:

- The minimum material requirements for an underwater HPES system deployed in waters up to a maximum depth of 200 m are obtained at pressure ratios between 2.4 and 2.7;
- Changes in sea depth and peak pressure shift the value of optimum pressure ratio;
- The length of PVs increases with sea depth, but decreases with higher peak pressures for a fixed energy storage capacity;
- The FLASC storage system has the minimum seabed footprint, but utilises more material than the seabed-mounted HPES systems, particularly in shallower waters.

ACKNOWLEDGEMENT

Project supported through the Maritime Seed Award 2019, a joint initiative between the Malta Marittima Agency (MMA) and the University of Malta supported by the TAKEOFF Business Incubator, Knowledge Transfer Office and the Centre for Entrepreneurship and Business Incubation (CEBI) at the University of Malta.

REFERENCES

[1] J. Lee, F. Zhao, A. Dutton, B. Backwell, L. Qiao, S. Lim, A. Lathgaralead and W. Liang, "Global Offshore Wind Report 2020, Global Wind Energy Council," Brussels, Belgium, 2020.

[2] "Equinor has installed Batwind - the world's first battery for offshore wind - equinor.com", Equinor.com, 2018. [Online]. Available: https://www.equinor.com/en/news/26june2018-equinor-has-installed-batwind.html. [Accessed: 10-Mar-2021].

[3] M. Puchta, J. Bard, C. Dick, D. Hau, B. Krautkremer, F. Thalemann and H. Hahn, "Development and testing of a novel offshore pumped storage concept for storing energy at sea - Stensea,"*Journal of Energy Storage*, vol. 14, pp. 271-275, 2017.

[4] A.J. Pimm, S.D. Garvey and M. De Jong, "Design and testing of Energy Bags for underwater compressed air energy storage," *Energy*, vol. 66, pp. 496-508, 2014.

[5] FLASC, *Renewable Energy Storage - FLASC*, *FLASC*. [Online]. Available: https://www.offshoreenergystorage.com/. [Accessed: 18-Feb-2021].

[6] European Norm, "Unfired Pressure Vessels – Part 3: Design," European Standard, SM EN 13445-3:2014, 2014.

[7] Directive 2014/68/EU of the European Parliament and of the Council of 15 May 2014 on the harmonisation of the laws of the Member States relating to the making available on the market of pressure equipment, *Official Journal of the European Union*, Brussels, Belgium, 2014.

[8] D. Moss and M. Basic, *Pressure Vessel Design Manual*, 4th ed., Oxford, UK: Elsevier Inc., 2013.

[9] American Petroleum Institute, "Specification for Line Pipe, API Specification 5L," 43rd Edition, 2004.

[10] "Live Access Server," [Online]. Available: http://data.nodc.noaa.gov/las/getUI.do. [Accessed: 1-Mar-2021].

[11] "Hywind - leading floating offshore wind solution - equinor.com", Equinor.com. [Online]. Available: https://www.equinor.com/en/what-we-do/hywind-where-the-wind-takes-us.html. [Accessed: 22-Mar-2021].

[12] "Smaller Circles within a Larger Circle", Engineeringtoolbox.com. [Online]. Available: https://www.engineeringtoolbox.com/smaller-circles-in-larger-circle-d_1849.html. [Accessed: 22-Mar-2020].

[13] P. Koebe, "Kontaktprobleme der Konformen Abbildung," *Journal of Mathematical Physics*, vol. l, no.88, pp.141-164, 1936.

[14] D. Buhagiar, T. Sant and R.N. Farrugia "Marine Testing of a Small-scale Prototype of the FLASC Offshore Energy Storage System," *in the 6th Offshore Energy and Storage Summit*, Brest, France, 2019.

[15] C. Cutajar, T. Sant, R.N. Farrugia and D. Buhagiar, "Assessing the Impact of Integrating Energy Storage on the Dynamic Response of a Spar-type Floating Wind Turbine," *in the ASME 2nd International Offshore Wind Technical Conference*, St. Julian's, Malta, 2019.